Journal of the European Ceramic Society **18** (1998) 871–877

PII: S0955-2219(97)00175-1
0955-2219/98/$19.00 + 0.00

Thermodynamic Assessment and Experimental Check of Fluoride Sintering Aids for AlN

G. M. Gross, H. J. Seifert and F. Aldinger

Pulvermetallurgisches Labor, Max-Planck-Institut für Metallforschung and Institut für Nichtmetallische Anorganische Materialien, Universität Stuttgart, Heisenbergstr. 5, D-70569, Stuttgart, Germany

(Received 13 September 1997; accepted 26 September 1997)

Abstract

This paper describes a theoretical and experimental access to new sintering aids for the densification of aluminium nitride and the prediction of its behaviour during sintering, using thermodynamic assessments. Based on thermodynamic calculations using Thermo-Calc software and the attached database SGTE, sintering aids like Ca, Y and some rare earth containing compounds were assessed and secondary phases were determined. Predictions were confirmed by experiments. © 1998 Elsevier Science Limited. All rights reserved

1 Introduction

Aluminum nitride has been stated a very promising ceramic material for electronic substrates due to its high thermal conductivity, along with good electrical and mechanical properties.[1] In the meantime, the production of such components by densification of AlN powder has been attempted by various techniques in the past decade.[2]

As compared to single crystals [$\lambda = 320$ W/(mK)],[3] its thermal conductivity in polycrystalline ceramics, however, is decreased by grainboundary phases, porosity, and impurities dissolved within the AlN crystals.[4–6] In polycrystalline material the highest attained value was 280 W/(mK).[7]

The most detrimental effect is caused by oxygen impurities incorporated by defect reaction:

$$3(1-x)\mathrm{AlN}+x\mathrm{Al_2O_3} \leftrightarrow (\mathrm{Al_{3-x}Va_{Al}})(\mathrm{N_{1-x}O_x})_3 \quad (1)$$

Oxygen occupies nitrogen sites ($O_N^{\bullet}$), creating a single aluminum vacancy (Va_{Al}''') for each three oxygen atoms for charge compensation.[8] Mass difference due to the aluminum vacancy is the major contributor to the scattering of phonons which results in the decrease in thermal conductivity.[9] This unfavourable influence of oxygen defects can be minimised using specific sintering aids, as will be described in the following:

1. to achieve the liquid state at temperatures less than 1800°C and to promote densification through liquid phase sintering;
2. to act as a gettering agent by incorporating oxygen and other impurities into the liquid phase; and
3. to form secondary phases with impurities.

A variety of additives has been used like Ca compounds for liquid phase sintering of pure AlN to achieve densities near 3·26 g m^{-3} and to improve the properties of the ceramic.[10,11] It was reported that sintering temperature could be decreased from 2000 to 1600°C using a mixture of CaO, SiO_2 and Al_2O_3, but within thermal conductivity (λ) decreased to 70 W/(mK).[12] High λ values of about 280 W/(mK) could be achieved after sintering and annealing the samples at 1800°C for 24 h.[7] Experiments show that Ca and Y compounds form aluminates that could incorporate oxygen impurities.

The aim of the present work was to develop new routes for the sintering of AlN by testing different sintering aids, theoretically and experimentally and to produce thus a dense ceramic at low sintering temperatures achieving thermal conductivity higher than 100 W/(mK). Therefore the choice of Ca and Y compounds was improved using thermodynamic assessment. Rare earth compounds were applied due to their chemical similarity to Ca compounds.

2 Thermodynamic Calculations

Thermodynamic calculations which are documented in numerous standard textbooks on thermo-

dynamics,[13] were carried out in order to predict possible phase reactions during the sintering process. Assuming the general reaction

$$\nu_1 A_1 + \nu_2 A_2 + \ldots\ldots = \nu_I A_I + \nu_{II} A_{II} + \ldots\ldots \quad (2)$$

the reaction isotherm according to van't Hoff

$$\Delta_R G = \Delta_R G^0 + RT[\ln(p_I^{V_1} \cdot p_{II}^{V_{II}}) - \ln(p_1^{V_1} \cdot p_2^{V_2})] \quad (3)$$

is used to analyse whether Δ_{RG} is positive no reaction or negative reaction is possible. The partial pressures p_i are exchanged by activities a_i in case of condensed phases. The Gibbs energy functions can be analytically described with the following expression:

$$G - H^{SER} = m_1 + m_2 \cdot T + m_3 T \cdot \ln(T) + m_4 \cdot T^2 + m_5 \cdot T^3 + m_6 \cdot T^{-1} + \ldots\ldots \quad (4)$$

where SER = standard elements reference, i.e. the enthalpies of the pure elements in their defined reference phase at 298·15 K.

The analytical descriptions on the Gibbs energy functions for all phases and gas species taking part in the reaction as derived from the SGTE database[14] are shown in Table 1. Thermodynamic calculations were done for $\Delta_R G$ using the program Thermo-Calc.[19]

3 Experiments

Base mixtures of aluminum nitride Grade F (Table 2) and 1, 3, 5 and 8 mass% of fluorides of calcium or rare earths, were prepared by attrition milling the mixtures in isopropanol. After drying powder mixtures were cold isostatically pressed with an applied pressure of 625 MPa into cylindrical green bodies (14×12 mm) achieving theoretical densities of about 64±6%. For each composition, five samples were fabricated.

The samples were pressureless sintered in a graphite crucible at 1600°C for 240 min and 1550°C for 130 min in a graphite heated resistivity furnace (Gero, Germany) in a 0·1 MPa nitrogen atmosphere. Heating rates of 2, 5 and 10 K min^{-1} were used. The actual temperature was measured using an infrared pyrometer up to 900°C and a quotient pyrometer at higher temperatures. After sintering the cylindrical samples were sectioned by sawing and the surfaces ground and polished for further investigations.

The density (ρ) of the sintered bodies was determined by the water immersion method. The thermal diffusivity (α) was measured using the xenon-flash method (Xenonplussystem XP 20, Compo Therm, Germany) at room temperature. Discs used for the thermal diffusivity measurements had a minimum diameter of 10 mm and thickness ranging from 1 to 2 mm. Samples were coated on both sides with a sprayed carbon layer to prevent direct transmission of the xenon-flash. The thermal conductivity (λ) was calculated from

$$\lambda = \alpha \cdot \rho \cdot C_P \quad (5)$$

The heat capacity C_P of AlN with yttrium oxide as sintering aid was given to 738 J/(kgK) AG Hoechst, pers. comm., 1993. The present crystalline phases were identified, using X-ray diffraction (XRD) with CuK$_{\alpha 1}$ radiation (Siemens D-5000

Table 1. Used thermodynamic expressions for Gibbs energy for temperature region of 298·15 to 3000 K (SER = Standard element reference)

Parameter	*T [K]*	*G (J mol^{-1}) formula units*	*Refs*
$G^{Al2O3}-H^{SER}$	298·15	$-1\,707\,351+448{\cdot}021T-67{\cdot}T\ln(T)-6{\cdot}747{\cdot}10^{-2}T^2+1{\cdot}4205{\cdot}10^{-5}T^3+9{\cdot}39{\cdot}10^5/T$	[15,16]
	600	$-1\,724\,886+754{\cdot}857T-116{\cdot}258T\ln(T)-7{\cdot}2257{\cdot}10^{-3}T^2$	
	1500	$-1\,772\,163+1053{\cdot}455T-156{\cdot}058T\ln(T)+7{\cdot}09{\cdot}10^{-3}T^2-6{\cdot}29{\cdot}10^{-7}T^3+1{\cdot}2367{\cdot}10^7/T$	
$G^{AlN}-H^{SER}$	298·15	$-345\,837+359{\cdot}862T-54{\cdot}309T\ln T+8{\cdot}56{\cdot}10^{-4}T^2+2{\cdot}326{\cdot}10^6/T-1{\cdot}26{\cdot}10^8/T^2$	[16]
$G^{Y2O3}-H^{SER}$	298·15	$-1\,962\,268+724{\cdot}466T-118{\cdot}042T\ln(T)-1{\cdot}03{\cdot}10^6T^{-1}+5{\cdot}10^{-7}T^3$	[17]
$G^{27R}-7G^{AlN}-G^{Al2O3}$	298·15	$382\,948-187{\cdot}033T$	[16]
$G^{Y3Al5O12}-2{\cdot}5G^{Al2O3}-1{\cdot}5G^{Y2O3}$	298·15	$-320\,000+36T$	[17]
$G^{YAlO3}-0{\cdot}5G^{Al2O3}-0{\cdot}5G^{Y2O3}$	298·15	$-72\,500+4{\cdot}2T$	[17]
$G^{Y4Al2O9}-G^{Al2O3}-2G^{Y2O3}$	298·15	$-21\,500+12T$	[17]
$G^{DyAl5O12}-2{\cdot}5G^{Al2O3}-1{\cdot}5G^{Dy2O3}$	298·15	$-190\,982+9{\cdot}6T$	[18]
$G^{DyAlO3}-0{\cdot}5G^{Al2O3}-0{\cdot}5G^{Dy2O3}$	298·15	$-29\,332+12{\cdot}8T$	[18]
$G^{Dy4Al2O9}-G^{Al2O3}-G^{Dy2O3}$	298·15	$-80\,079+25{\cdot}3T$	[18]
$G^{Gd3Al5O12}-2{\cdot}5G^{Al2O3}-1{\cdot}5G^{Gd2O3}$	298·15	$-147\,253+10{\cdot}2T$	[18]
$G^{GdAlO3}-0{\cdot}5G^{Al2O3}-0{\cdot}5G^{Gd2O3}$	298·15	$-23\,795+13{\cdot}6T$	[18]
$G^{Gd4Al2O9}-G^{Al2O3}-2G^{Gd2O3}$	298·15	$-65\,026+26T$	[18]
$G^{LaAlO3}-0{\cdot}5G^{Al2O3}-0{\cdot}5G^{La2O3}$	289·15	$-40\,393+8{\cdot}2T$	[18]

Table 2. Chemical analysis of AIN Grade F powder[a]

Oxygen content (mass%)	*Carbon content (ppm)*	*Silicon content (ppm)*
0·9	3·5	<9

[a]As provided by the supplier (Tokuyama Soda, Tokyo,

Diffractometer, Karlsruhe, Germany). The microstructures and grain boundary phases of the sintered samples were examined using a scanning electron microscope (SEM Cambridge Instruments, Cambridge, UK) equipped with both an energy- and wavelength-dispersive X-ray microanalyser.

Powdered ceramics were quantitative analyzed using hot gas extraction (TC-436, Leco Instr. Corp., St Joseph, MI, USA) to detect amounts of oxygen and nitrogen content, and atom emission (ICP-OES, Typ JY 70 Plus, Jobin Yven, Paris, France) was used for the detection of metal cations.

4 Results and Discussion

4.1 Thermodynamic data

The impurity with the most important influence on thermal conductivity is the oxygen content. Therefore, the reaction of fluorides considered as sintering aid with oxygen bounded in different forms relevant to the sintering of aluminum nitride has to be investigated. At first the reaction with adsorbed oxygen was taken into consideration:

$$LnF_3 + 1/2O_2 = LnOF + F_2 \quad (6)$$

since powder preparation increased oxygen content from 1 to 2 mass% and residual moisture was detected to be 1·3 mass%. Reaction with water vapour also have to be taken into consideration:

$$LnF_3 + H_2O = LnOF + 2HF \quad (7)$$

$$2LnOF + H_2O = Ln_2O_3 + 2HF \quad (8)$$

with Ln = Y, rare earth like La, Gd, and Dy.

According to literature the reactions of fluorides with water start at 700°C,[20] but no thermodynamic data are yet available for the LnOF compounds, hence estimations of forming aluminates are only reasonable using alternative reaction schemes.

First we consider the formation of oxides from corresponding calcium or rare earth fluorides:

$$CaF_2 + H_2O = CaO + HF \quad (9)$$

$$2LnF_3 + 3H_2O = Ln_2O_3 + 6HF \quad (10)$$

Calculations were performed for eqns (9) and (10) for Y, La, Gd and Dy compounds between 1500 and 1800 K (Table 3). The Gibbs energy changes $\Delta_R G$ are fairly positive and indicate no reaction between fluorides and water in this temperature range. Vapour pressures derived from eqn (3) finally suggest that oxides are formed in open system.

In a second step, the calcium, yttrium or rare earth oxides were assumed to react with alumina present at the surface of the aluminum nitride powder to the corresponding aluminates according to the following reactions:

$$CaO + xAl_2O_3 = CaAl_{2x}O_{3x+1} \quad x = 1, 2 \quad (11)$$

$$Ln_2O_3 + Al_2O_3 = 2LnAlO_3 \quad Ln = Y, La, Gd, Dy \quad (12)$$

$$3Ln_2O_3 + 5Al_2O_3 = 2Ln_3Al_5O_{12} \quad Ln = Y, Gd, Dy \quad (13)$$

Figure 1 shows calculated Gibbs energy changes $\Delta_R G$ of the formed aluminates and their evolution in the temperature range from 1000 to 2000 K. All lines are situated in the negative part of the y axis, in the mentioned temperature interval. Yttrium garnet, $Y_3Al_5O_{12}$, is the most stable compound, and its stability is increasing with increasing temperature, up to its melting point of 2213 K.[17] Conclusions for experiments were that a secondary aluminate phase should be formed between 1773 and 2073 K.

Table 3. Gibbs energy changes and HF vapour pressures for reactions according to eqns (9), (10) and different fluorides

Fluoride	*T(K)/(°C)*	*ΔG(kJ mol^{-1})*	*log(p_{HF}/p_0)*
CaF_2	1500/1227	214·80	−7·48
	1600/1327	194·41	−6·34
	1700/1427	174·69	−5·36
	1800/1527	155·77	−4·52
YF_3	1200/927	171·68	−7·47
	1300/1027	155·25	−6·23
	1400/1127	98·44	−3·67
	1500/1227	75·32	−2·62
LaF_3	500/227	246·12	−7·56
	600/327	215·92	−6·26
	700/427	190·19	−5·22
	800/527	165·16	−4·31
GdF_3	1200/927	174·45	−7·59
	1300/1027	136·82	−5·49
	1400/1127	99·92	−3·73
	1800/1527	−23·59	0·68
DyF_3	1200/927	147·82	−6·43
	1400/1127	75·41	−2·81
	1600/1327	19·06	−0·62
	1800/1527	−31·84	0·92

4.2 Densification and sintering

Amounts of 1, 3, 5 and 8 mass% of fluoride sintering aids with AlN were investigated. Sintering with heating rates of 2, 5 and 10 K min^{-1}, respectively, were compared for samples with 3 mass% YF_3 shown in Fig. 2. Densities of 76·55 and 96·6% for samples sintered with 2 and 10 K min^{-1}, respectively, show that neither a very low heating rate nor a very high one leads to dense ceramics. Densities near 100% are achieved using 5 K min^{-1}. The observed shrinkage and mass losses are in accordance with the calculated results and are due to the vapourization of the fluoride compound. This observation was predicted from the calculation. The increase of shrinkage of samples sintered with 10 K min^{-1} corresponds to a loss of mass of about 2 mass% during heating, and is not due to liquid phase sintering. According to these results an average heating rate of 5 K min^{-1} was applied to all following investigations.

Sintering experiments with LnF_3 (Ln = La, Gd and Dy) are compared using 8 mass% of the corresponding sintering aid. Figure 3 shows sintering rates versus time using a heating rate of 5 K min^{-1}. In samples with YF_3, GdF_3 and DyF_3 as sintering aids, sintering starts at 1290°C. Sintering maxima and temperature of these maxima are 1·6% min^{-1} at 1500 and 1520°C and 1·2% min^{-1} at 1490°C, respectively, to the fluoride. All samples achieve densities higher than 99%. Samples with LaF_3 as sintering additive start sintering at 1360°C, having a sinter maximum with 1·45% min^{-1} at 1510°C, and reaching a final density of 99·4%.

According to these sintering experiments it could be expected that dense ceramics can be produced with the chosen sintering aids between 1500 and 1550°C applying a heating rate of 5 K min^{-1}.

4.3 Chemical analyses and secondary phases

According to hot gas extraction measurements, the total oxygen amount in AlN powder increases from 0·9 mass% to approximately 1·47 to 2·35 mass% after attrition milling for 2·5 h with isopropanol (Tables 2 and 4).

Table 4 shows sample compositions with 5 mass% of different fluorides studied before and after sintering for 240 min at 1600°C. Samples with 5 mass% CaF_2, 5 mass% LaF_3 and 5 mass% DyF_3 show a decrease of about 40% in oxygen content. The decrease in samples with YF_3 and GdF_3 is about 18%. This decrease is caused by reaction of oxygen, and thus of Al_2O_3 with the atmosphere of the graphite furnace, forming volatile products according to:

$$Al_2O_3 + 3C + N_2 = 2AlN + 3CO \quad (14)$$

$$CaO + 2C + N_2 = CaCN_2 + CO \quad (15)$$

$$Ln_2O_3 + 6C + 2N_2 = 4LnN + 6CO \quad (16)$$

The phase fraction diagram for reaction (14) is shown in Fig. 4. With increasing temperature the Al_2O_3 and carbon fractions decrease (starting from 5 mol of atoms and 3 mol for atoms, respectively) and AlN is formed. The amount of gas phase increases from 0·2 mol of atoms (according to N_2) to 0·6 mol of atoms (according to 3 CO) at 2200 K.

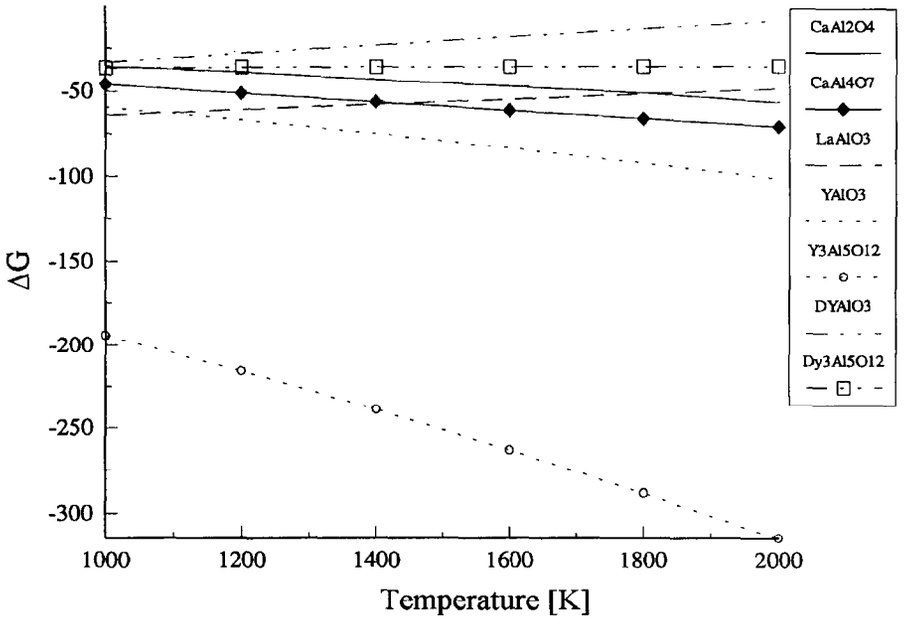

Fig. 1. Gibbs energy changes $\Delta_R G$ of the corresponding aluminates from CaO or Y-, Ln-oxides with Al_2O_3, [eqns (11)–(13)].

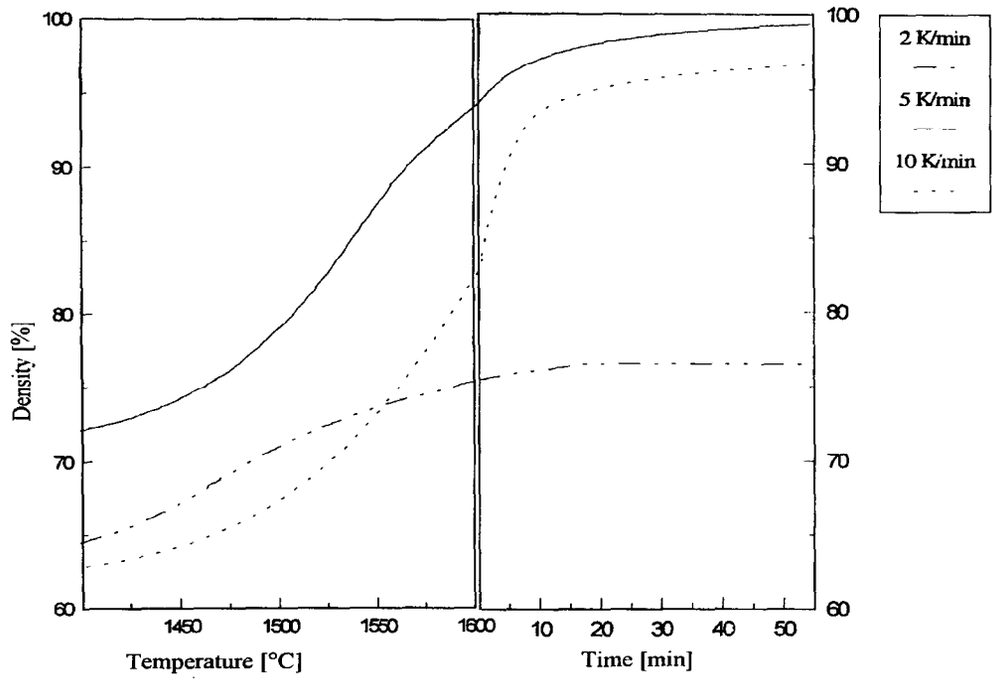

Fig. 2. Densities versus various heating rates as a function of sintering temperature and time at 1600°C (1873 K) for samples with 3·0 mass% YF_3.

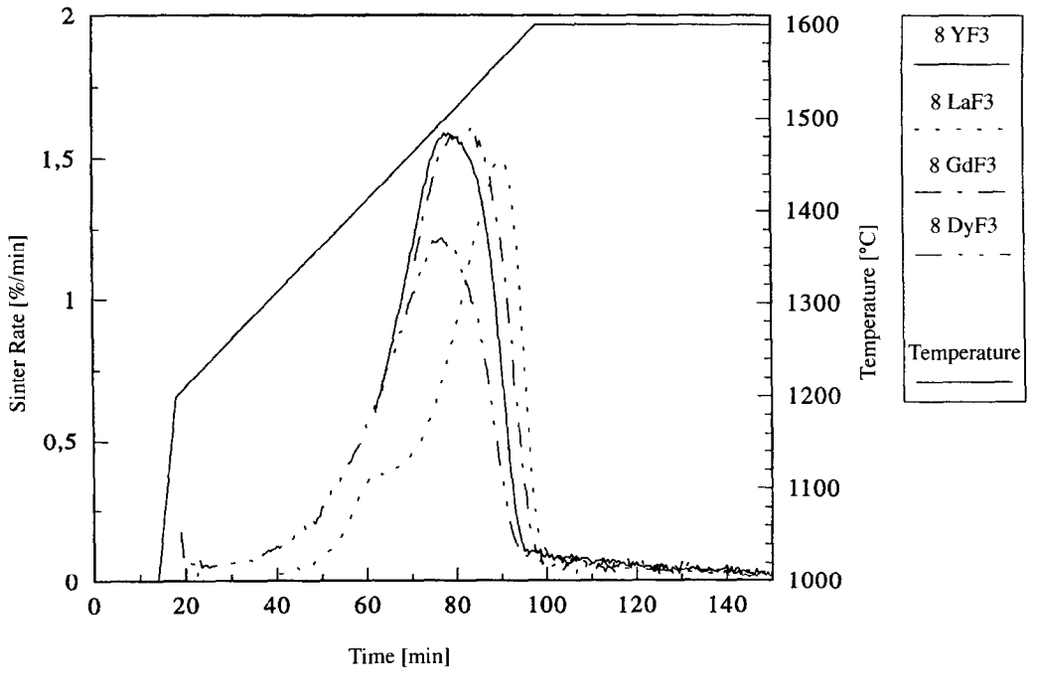

Fig. 3. Sintering rate versus sintering time for samples of 8·0 mass% LnF_3 heated at 5 K min^{-1} up to 1600°C (1873 K).

Table 4. Characteristic powder data of aluminium nitride with 5 mass% of different fluorides after attrition milling and after sintering for 240 min at 1600°C

	SSA after milling ($m^2\ g^{-1}$)	*Oxygen content after milling* (*mass%*)	*Oxygen content after sintering* (*mass%*)
CaF_2	7·7	2·35	1·37
YF_3	6·3	1·64	1·35
LaF_3	5·1	1·51	0·87
GdF_3	4·5	1·65	1·35
DyF_3	4·9	1·47	0·91

The crystalline phases identified by X-ray diffraction include AlN and the compounds listed in Table 5 for samples sintered for 130 min at 1550°C and for 240 min at 1600°C. Samples with CaF_2 are still containing some unreacted CaF_2 after sintering. It is interesting to note that samples sintered at 1550°C contain rare earth oxifluoride compounds and a perovskite type phase according to the applied sintering aid. Increasing the sintering temperature to 1600°C favoured the entirely formation of the aluminate phase. The oxi fluoride phase

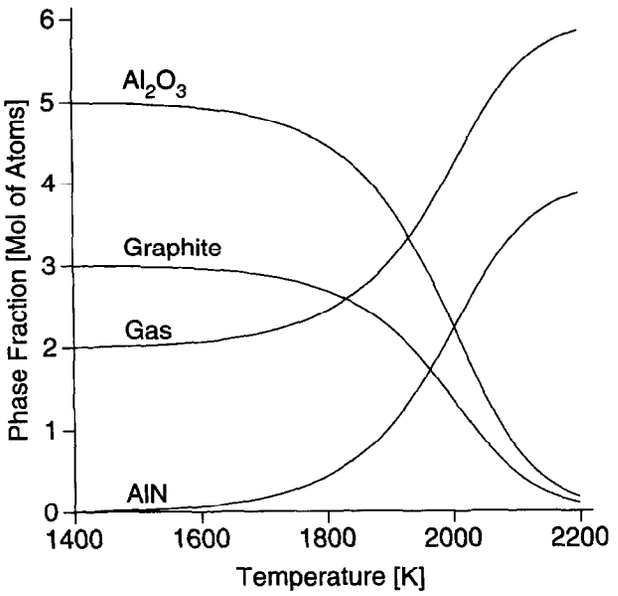

Fig. 4. Phase fraction diagram according to the carbothermal reduction (14) versus temperatures (K).

Table 5. Secondary phases in aluminium nitride with 5 mass% of different flourides after sintering at 1550°C for 130 min and 1600°C for 240 min.

	CaF_2	*YF_3*	*LaF_3*	*GdF_3*	*DyF_3*
1550°C/ 150 min	CA_2 CaF_2	$Y_3Al_5O_{12}$	$LaAlO_3$, LaFO	$GdAlO_3$, $Gd_4O_3F_3$[a]	$DyAlO_3$, $Dy_{1-x}O_xF_{1-x}$
1600°C/ 240 min	CA_2 CaF_2	$Y_3Al_5O_{12}$[a]	$LaAlO_3$	$GdAlO_3$	$DyAlO_3$

$CA_2 = CaAl_4O_7$.
[a]Unknown phase.

Table 6. Density, thermal diffusivity and thermal conductivity of aluminium nitride sintered with 5 mass% of different fluorides after sintering at different temperatures

	Sintering temperature (°C)/(K)	*Density (%)*	*Thermal diffusivity ($m\ s^{-1}$)*	*Thermal conductivity [W/(m·K)]*
CaF_2	1550/1823	99·1	2.67	63·8
	1600/1873	99·2	3·08	75·5
YF_3	1550/1823	100	3·37	82·6
	1600/1873	100	4·15	101·18
LaF_3	1550/1823	99·9	4·16	102·0
	1600/1873	99·5	4·50	111·3
GdF_3	1550/1823	100	3·47	86·4
	1600/1873	99·8	4·01	118·9
DyF_3	1550/1823	100	4·31	106·8
	1600/1873	99·8	4·42	109·4
		Error:	±0·05	±2·3

could not be detected at elevated temperature and time (Table 5). The identified crystalline phases are expected according to eqns (11) to (13). Oxifluoride phases detected after sintering at 1550° for 130 min, support the reaction scheme given in (6) to (8). Multicomponent phases of systems $AlN–Ln_2O_3–LnF_3$ or $AlN–Ln_2O_3$ have not been reported in literature and could not be detected in this work either.

4.4 Thermal conductivity

Thermal conductivities were calculated from thermal diffusivity measurements at room temperature from the samples of 5 mass% of varying fluoride aids (Table 6). Consistent results are obtained for those series of samples with CaF_2, YF_3, GdF_3 and DyF_3 sintered at 1550 and 1600°C (Fig. 5). Max-

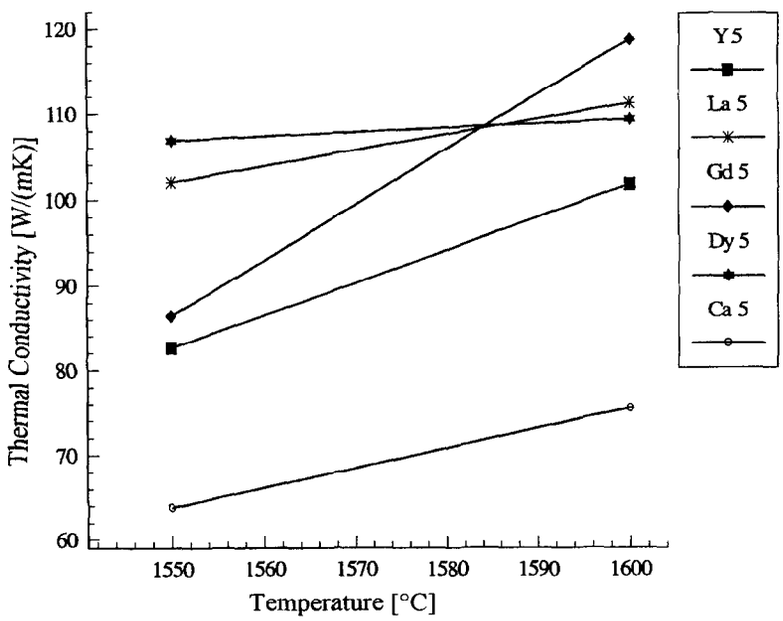

Fig. 5. Thermal conductivity versus sintering temperatures for samples with 5 mass% CaF_2, 5 mass% YF_3 and 5 mass% LnF_3 (Ln = La, Gd, Dy).

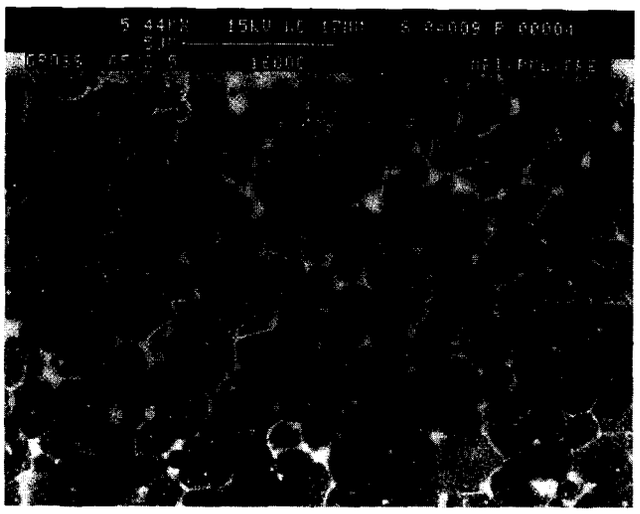

Fig. 6. SEM-photo of sample with 5·0 mass% GdF_3 after sintering at 1600°C (1873 K) and 240 min.

imum thermal conductivity is observed for samples sintered at 1600°C and is 34% higher than previously reported.[10] Increasing the sintering temperature by 50°C leads to an increase of about 25% for λ. Differences in thermal conductivity exist between samples with calcium fluoride and rare earth fluoride. Using calcium fluoride, thermal conductivity is reported to be highest with 75·5 W/(mK). In samples with YF_3, GdF_3 and DyF_3 as sintering aids, results that were obtained after sintering at 1600°C were exceeding 100 W/(mK) and reaching their maximum with 118·8 W/(mK) in samples with 5 mass% GdF_3. After sintering at 1550°C, thermal conductivities were of approximately 100 to 110 W/(mK) in samples using rare earth fluorides. Measurements on samples with fluoride sintering aids were 40% increased over those detected in samples with oxygen sintering aids, like CaO and SiO_2 sintered at the same temperature.[12] In samples with 5 mass% GdF_3 grain-boundary phases are located in the triple junctions of the AlN matrix and permits and direct contact of AlN grains (Fig. 6).

5 Conclusion

Thermodynamic assessment is suitable to predict the application of chemical compounds as sintering aids. In this work AlN was densified with Ca, Y, and rare earth fluorides. The predicted secondary phases were detected using X-ray diffraction. The indicated vaporisation of produced gaseous compounds was confirmed by mass losses.

After sintering with 5 mass% GdF_3 at 1600°C for 240 min, dense AlN ceramic was achieved with $\lambda = 118{\cdot}9$ W/(mK). Thermodynamic assessment in combination with experiments is a suitable tool to find sintering aids for the densification of AlN.

Acknowledgements

The authors are very grateful to Hoechst AG, Frankfurt/M. for enabling the measurements of thermal conductivity in its laboratory.

References

1. Werdecke, W. and Aldinger, F., Aluminium nitride—an alternative ceramic substrate for high-power applications in microcircuits. *IEEE Trans. Compon., Hybrides and Manuf. Technol.*, 1984, **7**(4), 399.
2. Ishizaki, K. and Watari, K., Oxygen behavior of normal and HIP sintered AlN. *J. Phys. Chem. Solids*, 1989, **50**(10), 1009–1012.
3. Slack, G. A., Nonmetallic crystals with high thermal conductivity. *J. Phys. Chem. Solids*, 1973, **34**, 321–335.
4. Koestler, C., Bestgen, H., Roosen A. and Boecker W., Microstructural development during sintering of AlN-Ceramics. 3rd ECSC, Madrid, Sept. 13–18, 1993.
5. Kuramoto, N., Taniguchi, H., Numata, Y. and Aso, I., Sintering process of translucent AlN and effect of impurities on thermal conductivity of AlN ceramics. *Yogyo Kyokai-Shi*, 1985, **93**(3), 517–522.
6. Udagawa, E., Makihara, H., Kamehara, N. and Niwa K., Influence of firing-gas pressure on the microstructure and thermal conductivity of AlN ceramics. *J. Mat. Sci. Letters*, 1990, **9**, 116–118.
7. Ueno, F. and Horiguchi, A., Grain boundary phase elimination and microstructure of aluminum nitride. *Proceedings of the 1st European Ceramic Society Conference (ECerS'89)*, 1989, **1**, 383–387.
8. Harris, J. R., Youngman, R. A. and Teller, R. G., On the nature of oxygenrelated defects in aluminium nitride. *J. Mater. Res.*, 1990, **5**(8), 1763–1773.
9. Abeles, B., Lattice thermal conductivity of disordered semiconductor alloys at high temperatures. *Phys. Rev.*, 1963, **131**(5), 1906–1911.
10. Jarridge, J., Mexmain, J. and Michelet, J. P., Sintering thermal diffusivity of AIN with fluoride additives. 2nd Europ. Ceram. Soc. Conf. (ECSC), Augsburg, 1991, pp. 1849–1853.
11. Horvath, S. F., Witek, S. R. and Harmer M. P. Effects of carbon and calcium oxide on the sintering behaviour of aluminium nitride. *Advances in Ceramics*, Vol. 26. The American Ceramic Society, Inc., Westerville, OH, 1989.
12. Streicher, E., Chartier, T., Boch, P., Denanot, M.-F. and Rabier, J., Densification and thermal conductivity of low-sintering temperature AlN materials. *Journal of the European Ceramic Society*, 1990, **6**, 23–39.
13. Gokeen, N. A. and Reddy, R. G., *Thermodynamics*, 2nd edn. Plenum Press, New York, 1996.
14. *SGTE Substance Database*, version 1996. SGTE, Domain Universitaire, BP66, F-38402 St Martin d'Héres, Cedex, France, 1996.
15. Taylor, K. M. and Lenie, C., Some properties of aluminium nitride. *J. Electrochem. Soc.*, 1960, **107**(4), 308–314.
16. Hillert, M. and Jonsson, S., Thermodynamic calculation of the Al–N–O system. *Z. Metallkd.*, 1992, **83**, 714–719.
17. Gröbner, J., Konstitutionsberechnungen im system Y–Al–Si–C–O. Ph.D Thesis, Universität Stuttgart, 1994.
18. Wu, P. and Pelton, A. D., Coupled thermodynamic-phase diagram assessment of the rare earth oxide–aluminium oxid binary systems. *J. Alloys and Comp.*, 1992, **179**, 259–287.
19. Sundman, B., Jansson, B. and Andersson, J.-O., Thermo-Calc databank system. *Calphad*, 1985, **9**, 53–190.
20. Banks, C. V., Burke, K. E. and O'Laughlin, J. W., *Anal. Chim. Acta.*, **19**, 1958, 239–243.